Journal Pre-proof

Electrochromic and colorimetric properties of anodic NiO thin films: Uncovering electrochromic mechanism of NiO

Dongmei Dong, Habiba Djaoued, Guillaume Vienneau, Jacques Robichaud, Delilah Brown, Ralf Brüning, Yahia Djaoued

PII: S0013-4686(20)30039-6

DOI: https://doi.org/10.1016/j.electacta.2020.135648

Reference: EA 135648

To appear in: *Electrochimica Acta*

Received Date: 7 August 2019

Revised Date: 19 December 2019

Accepted Date: 4 January 2020

Please cite this article as: D. Dong, H. Djaoued, G. Vienneau, J. Robichaud, D. Brown, R. Brüning, Y. Djaoued, Electrochromic and colorimetric properties of anodic NiO thin films: Uncovering electrochromic mechanism of NiO, *Electrochimica Acta* (2020), doi: https://doi.org/10.1016/j.electacta.2020.135648.

Electrochromic and Colorimetric Properties of Anodic NiO Thin Films: Uncovering Electrochromic Mechanism of NiO

Dongmei Dong [a], Habiba Djaoued [a], Guillaume Vienneau [a], Jacques Robichaud [a], Delilah Brown [b], Ralf Brüning[b], Yahia Djaoued [a,*]

[a] Laboratoire de Recherche en Matériaux et Micro-spectroscopies Raman et FTIR, Université de Moncton-Campus de Shippagan, NB, E8S1P6, Canada
[b] Physics Department, Mount Allison University, Sackville, NB, E4L 1E4, Canada

Abstract

In this work anodic NiO electrochromism is investigated under two potential cycling modes: i) the response between coloration and bleaching in increasing potential steps (switching); ii) the stepwise modulation to coloration with increasing potential and back to bleaching (modulation). The films' response is investigated by optical spectroscopy, colorimetry studies, Raman spectroscopy, XRD, cyclic voltammetry and chronoamperometry. Using the CIE (Commisson International de l'Éclairage) system of colorimetry the color stimuli of the films and the changes that take place upon reversible switching/modulation are recorded under various potentials. As shown by the CIE 1931 *xy* chromaticity coordinates, when NiO film is oxidized, a sharp decrease in luminance is observed. Optical measurements, performed as a function of applied potential, show excellent contrast between colored and bleached states. Up to now, for NiO, the coloration mechanism was considered as a surface phenomenon. Here, for the first time we show that upon ion insertion/extraction the lattice constant of NiO changes, proving that the EC coloration mechanism involves the unit cells in the bulk material. Furthermore, the fraction ratio of Li to Ni atoms ($\frac{Li}{Ni}$) is proposed. Considering the actual film fabrication conditions, the x value in Li_xNiO is found to be equal to 0.0046.

Keywords: Electrochromic; electrochromism; tungsten oxide; nickel oxide; coloration mechanism; colorimetry

*Corresponding author.
E-mail address: Yahia.djaoued@umoncton.ca

1. Introduction

Electrochromism is defined as a phenomenon in which a change in color takes place in the presence of an applied voltage and which involves the reversible insertion/de-insertion of ions within the film structure under electric potential [1]. There has been keen interest for years in research on electrochromic thin films due to their various applications. A step forward has been taken in the successful fabrication of films with excellent properties, even for commercial applications. However, the intrinsic mechanisms of electrochromic (EC) behavior sometimes still remain ambiguous. There has also been a strong interest for years in research on all-solid-state transmittance-type EC devices due to their various applications in ‘‘smart windows’’. A step forward has been taken in the preparation of full multilayered devices with enlarged optical contrast and fast switching response. As an anodically colored EC material, NiO has for a long time drawn attention to function as a counter electrode in a device, yielding brownish color with extraction of the cations.

However, the Li^+ intercalation mechanism is poorly understood for anodic NiO despite the fact that scientific inquiry has persisted for nearly 30 years [2]. In the work from A. Gorenstein et al. published in 1990 [3], a preliminary study on the EC property of NiO due to the intercalation of Li was carried out by cyclic voltammetry and by optical transmittance, but no deep insight into the mechanism of electrochromism was presented in this early paper. In the last five years, R. T. Wen has done great work concerning EC performance of Ni oxide thin films intercalated with Li^+ ions [4] as well as the decay of charge density upon extensive electrochemical cycling [5], but the question on what sites the intercalated Li ions reside was not solved. Besides, the EC property and the mechanism of NiO are researched in the group of A. Rougier in both Li-based electrolyte and Li free electrolyte [6]. The authors focus on the effect of nonstoichiometric feature of NiO thin films, that is, the presence of Ni^{3+}, on the EC performance. The Li intercalation sites are not the main topic, either.

Not only does the cause of the coloration/absorption for NiO remain unsettled but even the ionic species in redox reactions are sometimes much more unclear. The issues become even more difficult in the case of lithium salt organic electrolytes than those in

KOH solutions [7,8]. The inability to keep its color for a long time (poor memory effect) also imposes challenges in understanding the origin of NiO coloration. It has been argued that, the coloration reaction occurring in NiO films only limits to the surface, mainly the outer parts of the grains [9]. But paradoxically, based on the work of Lampert et. al. [10], the active sites for coloration/bleaching behavior of NiO in KOH solution are not likely at the surface, but within the NiO bulk. Most EC devices for practical applications use cathodic WO_3 thin films separated from anodic NiO films by electrolytes in thin-film-forms or as polymer layers. This sandwich-like configuration is embedded between transparent conductive electrodes. Hence, to realize the commercialization of a complete WO_3//NiO device, a better understanding of the nature of charge insertion/extraction involved in cycling as well as the difference in the working mechanisms for the two films is required.

This paper reports on a comprehensive investigation of anodic NiO films cycled in a Li^+-based electrolyte, $LiClO_4$-PC. The EC behavior of the films was investigated under two different cycling potential modes: i) the switching response between coloration and immediate bleaching in increasing potential steps (switching); ii) the gradual modulation to coloration with increasing potential steps and back to bleaching (modulation). Also, for the first time the lattice constant and diffraction line width show that the EC NiO coloration mechanism is not limited to the crystalline surface. We found a tight correspondence between color switching/modulation and intrinsic micro-structure evolution in the NiO films. The inside of NiO grains is involved in the process of charge insertion/extraction. Moreover, we estimated the fraction ratio of lithium to nickel atoms ($\frac{Li}{Ni}$) and found that x in Li_xNiO is ~0.0046.

2 Experimental

2.1 Fabrication of NiO thin films

For all the deposition techniques, the electrochromic properties are strongly sensitive to the deposition parameters, and this in turn means that the same compound with different microstructures can present different electrochromic responses.

Anodic NiO films were prepared via a reactive direct current magnetron sputtering

technique, in which the contamination was greatly reduced under vacuum condition. The thickness of the film was carefully controlled, and the morphology, stoichiometry and structure can be realized by adjusting the series of deposition parameters [11,12].

NiO films were deposited using reactive direct current magnetron sputtering technique from nickel metallic target (60 mm diameter and 3 mm thickness in size; purity: 99.9%) in a mixture of oxygen (purity: 99.99%) and argon (purity: 99.99%) gas onto 5 × 5 cm^2 commercial ITO glass substrates (T% = 85%; sheet resistance 30Ω/Sq) at room temperature. The separation of target to substrate was 17cm. Before film deposition, the chamber was evacuated to a base pressure below 3.0×10^{-3}Pa by a turbo molecular pump combined with a rotary pump. The flow rates of argon and oxygen gas was individually set by mass flow controllers. To improve the film uniformity, the holder was rotating on its symmetry axis at a constant speed. During deposition, the system pressure is maintained to 2.4Pa for NiO films. Film thicknesses were measured to be ~400 nm, using a step profiler (Dektak II, Bruker Corp., Germany). For comparison purposes, cathodic WO3 was also was also prepared. More details on the optimized deposition parameters of the films are gathered in Table 1.

Table 1 Detailed deposition parameters of the NiO and WO_3 films.

Target	Power source	Pressure (Pa)	Ar: O_2	Power (W)	Time (min)	Thickness (nm)
Ni	DC	2.4	200:3	320	50	400
W	DC	1.7	200:80	480	50	500

2.2 Fabrication of the electrolyte

Prior to cycling the EC NiO films, a 1M $LiClO_4$ Propylene Carbonate (PC) ionic liquid electrolyte was prepared with $LiClO_4$ powder (99.9% purity) and analytical-grade PC purchased from Sigma-Aldrich. Both were mixed at room temperature and stirred for half an hour to obtain a uniform transparent solution.

2.3 Switching and modulation cycling modes

The as-deposited NiO films were cycled in two different modes: switching and

modulation. In this work, “switching” refers to the sample being colored and bleached at inverse potentials, step by step. For example, the potentials were applied in the following sequence: 0, +0.5, -0.5, +1.0, -1.0, +1.5, -1.5, +2.0, -2.0, +2.5, -2.5, +3.0, -3.0 V. As for the “modulation” cycling mode, the films were gradually colored by varying the potential from 0 to +3.0 V, in steps of +0.5 V and then bleached by inverting the potential from 0 to -3.0 V, in steps of -0.5 V. For better understanding of anodic NiO electrochromism, synchronous contrast experiments were also done on cathodic WO_3.

2.4 Characterization

The optical, structural and morphological properties of the films were investigated after every coloring or bleaching step. Prior to measurements, the films were washed with deionized water to remove any trace of the electrolyte (Propylene-Carbonate $LiClO_4$) and then dried. The colored/bleached films are processed following the same steps, in order to be comparable for the analysis.

The optical transmission and absorbance spectra of EC films were recorded using a Biochrom Ultrospec 2000 UV-vis-NIR spectrophotometer. Color measurements were performed using a MiniScan EZ spectrophotometer from HunterLab. X-Ray Diffraction (XRD) was carried out in reflection with a custom-built θ-θ diffractometer equipped with pyrolytic graphite monochromator and analyzer crystals. Cu-Kα radiation with wavelength λ =0.154 178 nm was used for the measurements, and the data are shown as a function of the modulus of the scattering vector $q = 4\pi\lambda^{-1}\sin\theta$, where 2θ is the scattering angle. Air-scattering was avoided by evacuating the sample space. Raman Spectroscopy was recorded at room temperature with a Jobin-Yvon Labram HR micro-analytical spectrometer using a 633nm laser filtered to give ~1.5mW at the sample surface. The spectra were generated with an 1800 grooves/mm grating across the 0.8 m length of the spectrograph giving a resolution estimated to be less than 0.5 cm^{-1} for a slit width of 150 μm and a confocal hole of 300 μm. After the immersion and drying steps and before Raman measurements, we took pictures of the films over a white background quickly at the same positions and with the same parameters using a Canon camera (4.3 V; PC 1743; No. 492172002247; N118; Canon Inc. made in Japan). All electrochemical measurements were carried out at room temperature in a three-electrode cell of

conventional design. Platinum grids served as counter electrode, whereas the reference was a commercial Ag/AgCl 1 M KCl electrode.

3. Results and discussion

3.1 Optical Properties

The spectral properties of NiO films were investigated in colored and bleached states by applying a step potential for 60 s in a $LiClO_4$-PC electrolyte. The results of the spectral transmission of the films after cycling in the switching and modulation modes are presented in Fig. 1. The transmittance of NiO decreases due to oxidation of Ni^{2+} to Ni^{3+}. At fully colored and bleached states in modulation response, the optical contrast at a wavelength of 550 nm can reach ~40% for NiO. Specifically, at 3.0 V, the bleached transmittance exceeds 80% at 550 nm, while the colored transmittance is below 50%. In switching, the transmittance shows an obvious drop from 67.1% to 49.9% as the potential step increases from +2.5 V to +3.0 V; in modulation, when the potential varies from +2.0 V to +2.5 V, the transmittance is changing from 56.4% to 48.6%. Thus, NiO can contribute to the transmission adjustment and can function as counter electrode in a full device. In addition, it is noteworthy that in coloration state, as compared to switching, modulation will provide an even lower transmittance at the same potential, for which the consecutive charge accumulation should be responsible.

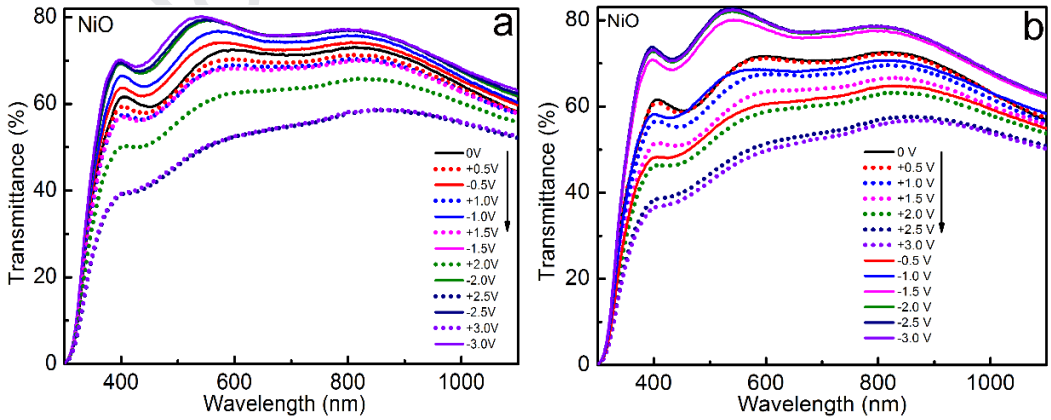

Fig. 1. Switching (a) and modulation (b) transmittance spectra of NiO films in response to applied potentials ("+" correlates to coloration and "-" to bleaching). Solid line: bleached state; Dotted line: colored state. The experimental sequence of applied potentials is indicated by a vertical arrow to the right of the legend.)

The optical band gaps (E_g) of NiO (Fig. 2) at initial/colored/bleached states are

calculated by applying the well-known Tauc model [13-16]. The typical plots of $(\alpha hv)^2$ versus hv is expected to show a linear behavior for direct transition in the region of strong absorption, i.e. near the fundamental intrinsic absorption edge, where α is the absorption coefficient and hv is the photon energy. The correlation coefficient R^2 for the linear fitting is about 0.98. The E_g values are evaluated by extrapolating the linear fitting portion to the photon energy axis and are found to be variable in the EC process. The E_g values of initial/colored/bleached states for NiO are calculated to be 3.900±0.008/3.874±0.007/3.930±0.008 eV, respectively. It is clearly seen in coloration that E_g decreases for NiO but increases for WO_3 (see Fig.S3), which corelates to their corresponding redox reactions and changes in valence states. To become colored, Ni^{2+} lose electrons to increase its valence state while W^{6+} ions need to gain electrons. The initial color of NiO films (brown) is between bleached (light brown) and colored state (dark brown). Thus, the colored and bleached band gaps of NiO are at different sides of the initial optical band gap.

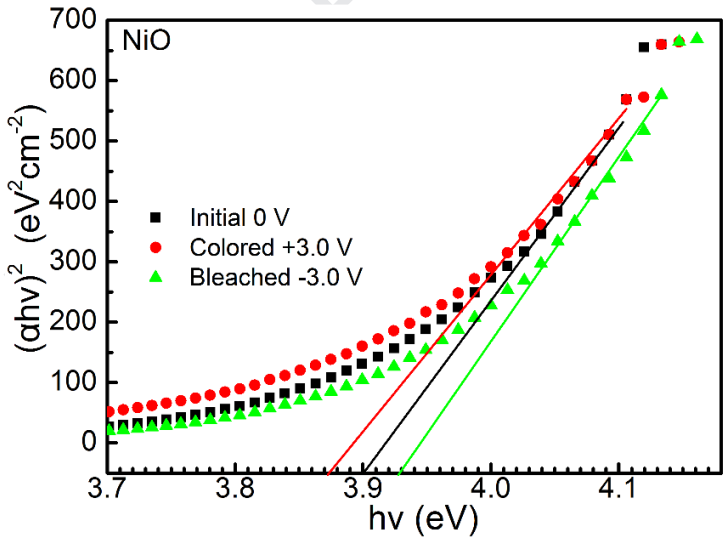

Fig. 2. Tauc plots of NiO films at initial and fully colored and bleached states.

3.2 Colorimetric studies

Chromaticity is a key indicator for quantitative evaluation of the color variation. The CIE 1976 L*a*b* color space is used to assess the color difference dependent on potential (Tables S1 to S4), in which L* stands for the lightness ranging from 0 to 100, a* stands for the degree of red versus green, and b* represents yellow versus blue [17,18].

The dynamic variation of the CIE 1931%$Y_L xy$ chromaticity coordinates for one film as a hue and saturation track as a function of the magnitude and direction of the applied voltage is studied (Fig. 3).

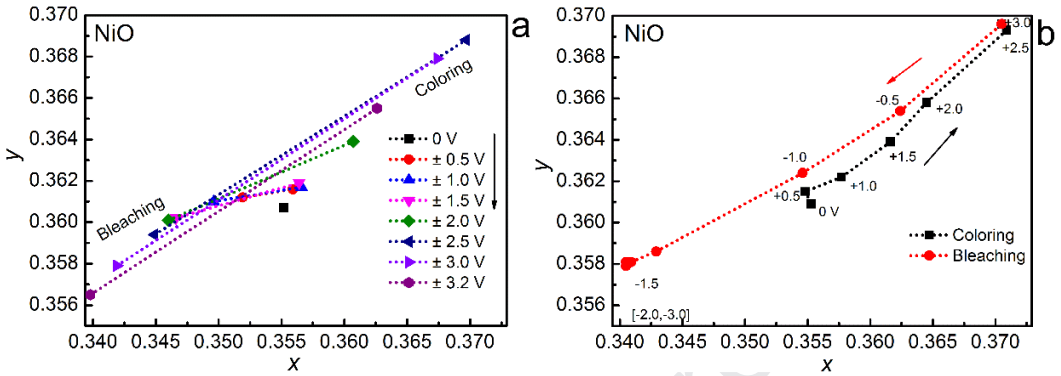

Fig. 3. CIE 1931 *xy* chromaticity plots for NiO films in switching (a) and modulation (b) response.

With increasing potential, the *xy* position of the NiO film separates from the initial state. When the potential value is too high, exceeding 2.5 V, no siginificant change will take place in *xy* values, which is a sign of approaching the critical potential and the maximum change for the film. The EC anodic NiO and cathodic WO_3 behave in opposite ways regarding to the *xy* variation trend (see Fig.S4). For WO_3 the *x* and *y* coordinates first decrease during coloration and then increase during bleaching, while for NiO, the coordinates increase during coloration and decrease during the following bleaching. As mentionned before, NiO and WO3 are often included as two functional layers in the fabrication of a full EC device. Hence, the color balance, or the color neutrality gained from the combination of WO_3 and NiO is an obvious advantage. The *xy* data for WO_3 and NiO EC-modulation response are overlaid onto the CIE 1931 color space template (Fig.4), showing the track of *xy* coordinates evolving steadily from coloration to bleaching. At the initial state of 0 V, the films are relatively transparent and their positions on the chromaticity plot are near to the white point. On stepping to negative potential, WO_3 turns blue with a dominant wavelength $\lambda_{d\text{-}WO_3}$ of 461 nm, which can be obtained by drawing a straight line from the white point through the point of fully colored state to the spectral locus. For NiO at colored state, the dominant wavelength $\lambda_{d\text{-}NiO}$ is estimated to be 583 nm after positive potential cycling. Although it might be expected that the combination of *xy* pair and corresponding dominant wavelengths would result in orange, in combination with low luminance (Fig. 5), the NiO films are still perceived as

dark brown. In the chromatic space, the coordinates of WO_3 and NiO in EC modulation move in opposite directions relative to the white point, contributing to the color balance or neutrality of an EC device incorporating WO_3 and NiO films.

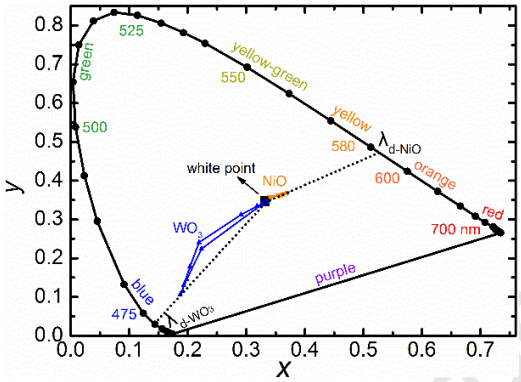

Fig. 4. CIE 1931 *xy* Coordinates for anodic NiO and cathodic WO_3 films in potential dependent modulation response. The locus coordinates together with hue wavelengths and corresponding colors, as well as the evaluation of the dominant wavelength ($\lambda_{d\text{-}WO_3}$=461 nm, $\lambda_{d\text{-}NiO}$=583 nm) of the deep blue state of colored WO_3 and dark brown of colored NiO, respectively, are shown in this plot.

The relative lightness or darkness of a color, represented by relative luminance, is an important dimension of how it is perceived [19]. Since it is not included in the CIE color space diagram, we present the relative luminance data *vs* potential of our NiO samples (Fig. 5). The colorimetric luminance correlates with the applied potential. For WO_3, as the blue color is getting dark, both a* and b* values are becoming more negative (Table S1 & S2), in contrast, their values are changing in a more positive direction for NiO. Concurrently, on switching, the luminance values jump up between "negative" and "positive" potentials (Fig. 5a), and change monotonically upon modulation (Fig. 5b). On potential cycling, the relative luminance difference between colored and bleached states is nearly 35% for NiO films.

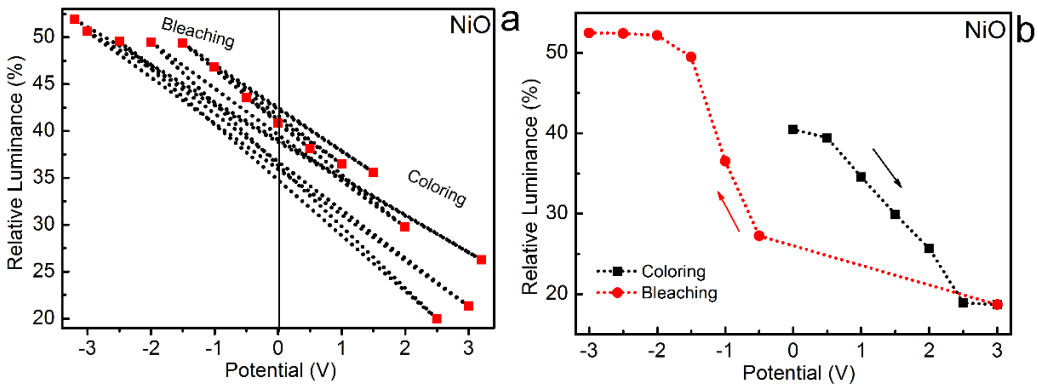

Fig. 5. CIE 1931 relative luminance data *vs* potential for NiO films in (a) switching/(b) modulation response. Data points are joined by straight lines for clarity.

3.3 Intrinsic structure evolution

3.3.1 Raman studies

Raman measurements are applied to monitor the structure evolution of NiO based films during switching (Fig. 6) and modulation (Fig. 7) processes. In the 100-1300 cm^{-1} wavenumber range, the characteristic peaks of the NiO phase are clearly present [20,21]. First-order Transverse Optical (1TO) and Longitudinal Optical (1LO) phonon modes are located at 400 and 520 cm^{-1} respectively. Second-order TO+LO phonon mode is around 926 cm^{-1} and 2LO is near 1080 cm^{-1}.

Stoichiometric cubic or rhombohedral NiO does not show first-order Raman scattering (1TO and 1LO) [22-25]. In this work the disorder-induced first-order band has high intensity, which is caused by symmetry-breaking imperfections such as nickel vacancies, interstitial oxygen, surface effects or disorder in the crystal lattice [26-28]. The intensity of the first-order band increases with potential during coloration, indicating the creation of more nickel vancancies brought about by the reduction of NiO. As shown in the zoom view (Fig. 7 left), there is a shift to lower energies (red shift) in the LO peak position as the brown color gets darker with increasing potential. This prominent peak moves towards the opposite direction (blue shift) after applying a negative potential, accompanied by less saturation in the film. With potential increasing, the peak returns back to its initial position. When the potential increases up to +3.0 V, the 512.8 cm^{-1} peak shifts to 496.9 cm^{-1} thereafter, the peak is shifted back as the potential switches to negative from +3.0 V to -3.0 V. This peak has been identified as Ni-O vibration [29]. We conclude that the red shift in coloration is associated with the oxidation of Ni^{2+} to Ni^{3+}. The structure with Ni^{3+} accompanied by vancancy defects is less defined than pure $Ni^{2+}O$; and therefore, the energy for exciting Ni-O vibration is smaller, leading to the red Raman shift.

Figures 6 & 7 show a prominent peak around 500 cm^{-1}, arising from one–phonon scattering in fcc-NiO [30,31]. A shoulder at 400 cm^{-1} (1TO band) becomes less pronounced in coloration and appears after applying even a small bleaching potential.

The decrease of the 1TO band during coloration arises from the oxidation of Ni^{2+} to Ni^{3+} together with disorder induced by defects or surface effect. This shoulder is associated with hydroxide bands [32]. A small new peak at 926 cm^{-1} appears upon coloration and disappears upon bleaching. The appearance of this peak is attributed to second-order Raman scattering (2TO+2LO) [33], which can be associated to Ni-O bonding. The 2TO+2LO peak centered at 926 cm^{-1} could be attributed to the stretching vibrational modes involving Ni^{3+}=O and Ni^{3+}-O sites. At the end of the coloration process, as the potential switches from +3.0 V to –0.5 V, the shoulder at the low energy side of the prominent peak increases in intensity; in sharp contrast, the peak at 926 cm^{-1} vanishes gradualy, becoming undetectable when the potential is below -1.5 V. Another peak centered around 1080 cm^{-1} (2LO band) becomes more pronounced in bleaching than in coloration.

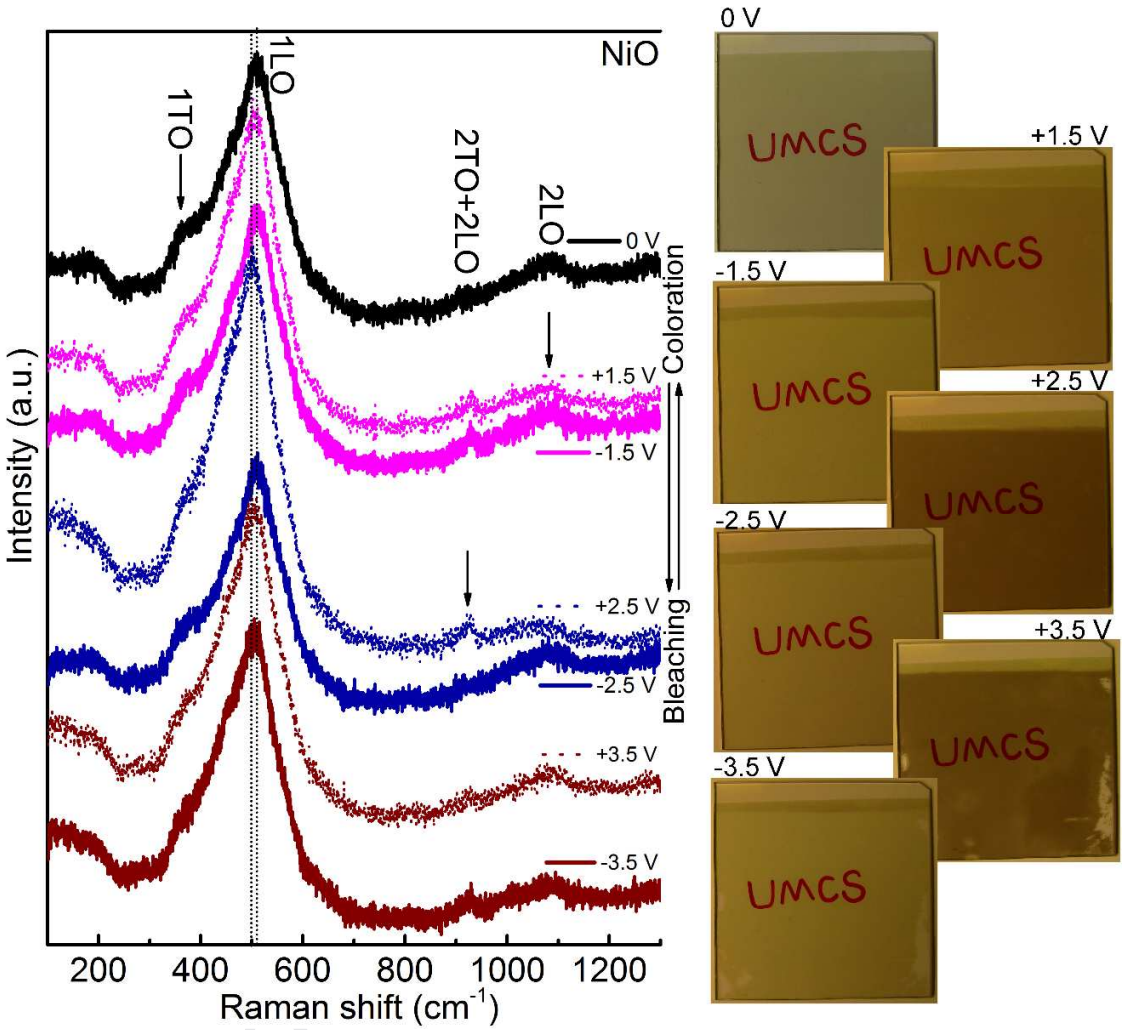

Fig. 6. Raman spectra of NiO in switching response. All curves were obtained with the same film; the arrows on the right side represent the experimental sequence.

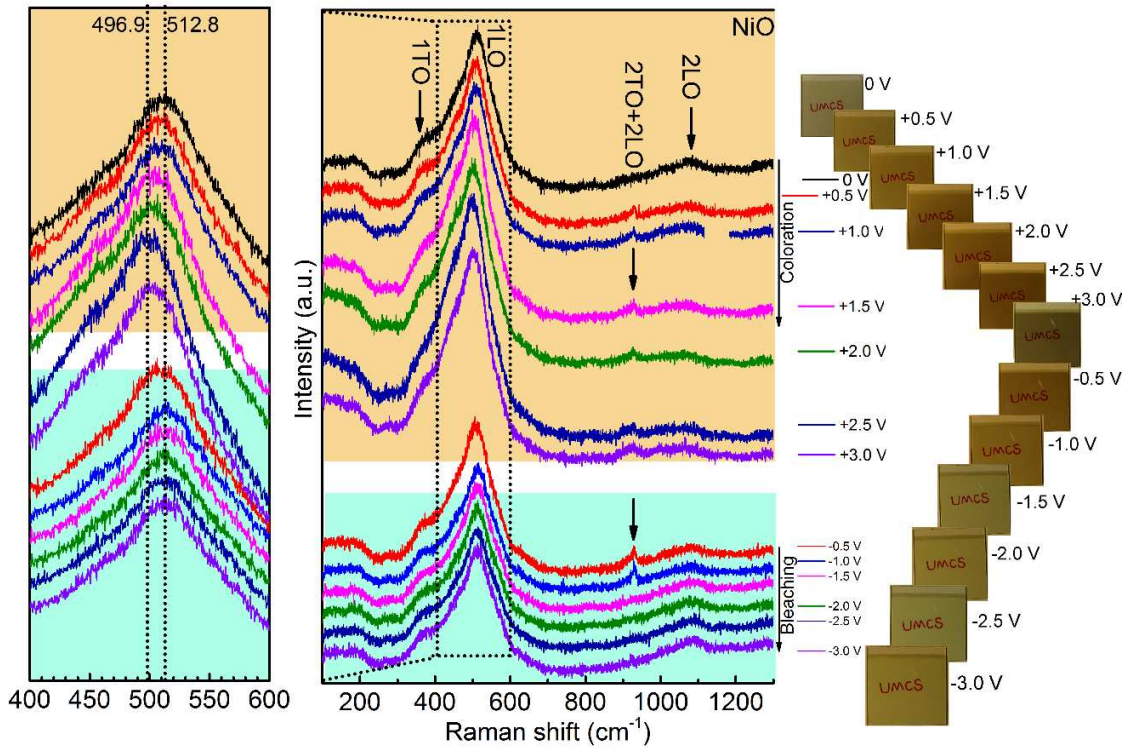

Fig. 7. Raman spectra of NiO in modulation response in 1M PC-$LiClO_4$ electrolyte at various potentials, together with corresponding digital photographs. The spectra are vertically shifted for clarity. (Coloration/bleaching time: 60 s). *The egg shell and turquoise cbackground colors refer to the colored and bleached states of the films, respectively.

3.3.2 Microscopic structure analysis

The SEM images in Fig.8, illustrate how the dynamics of the EC process influences the NiO films surface micro-structure at different coloration/bleaching stages during switching (Fig.8a) and modulation (Fig.8b). At the initial 0 V state, the films are relatively porous and with increasing potential no significant morphological change is observed. As measured from the SEM images using ImageJ software, the crystallite sizes of NiO, colored/bleached at 0 V, ±1.5 V and ±3.0 V in the switching process, were estimated to be ~ 8.0 to 9.0 nm. These results are partly exhibited in Tables S5 to S9 of the Supplementary Information.

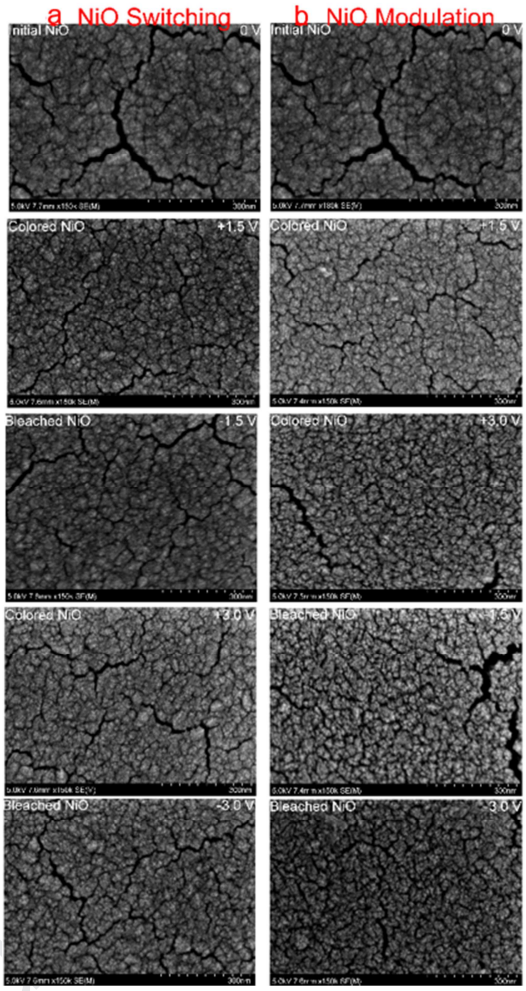

Fig. 8. SEM images of NiO films showing no significant morphology evolution during switching(a) and modulation (b).

3.3.3 XRD analysis

XRD was performed on the NiO film during switching and the grain size and lattice constant calculations were carried out. The XRD patterns (Fig. 9a) for the film colored and bleached at 0, ±2.0, ±2.5, ±2.5 and ±3.0 V were taken from the same area on the sample. Here, the stability of the ITO electrode, working within the potential window -3.0 to +3.0 V is indicated by the unchanged intensities of the substrate diffraction peaks at about 35, 36, 42, 45 and 60 degrees. The NiO layer is crystalline fcc-NiO with diffraction peaks from the (111), (200) and (220) lattice planes (JCPDS No. 47-1049). The (220) and (111) are strong reflections, whereas the (200) diffraction intensity is low relative to the powder diffraction reference intensities. This shows that the crystallites in the film have a

preferred orientation such that their [110] and [111] directions are aligned with the normal of the film's surface. The XRD peaks are fitted with pseudo-Voigt functions and line shape parameters for calculation of the lattice constant and crystallite size, between 0.85 to 1.0. The fits are shown by the red lines in Fig. 9a. They are somewhat hard to see because they coincide very closely with the experimental data. In fitting the data, we described first the signal originating from the ITO/glass substrate. This background signal is modeled by the sum of a broad third-order polynominal and pseudo-Voigt peaks, the latter corresponding to the ITO film. The NiO gives rise to three additional peaks corresponding to the 111, 200 and 220 interplanar spacings. For each state of the film, these three peaks were fitted with a single lattice constant and a single peak width, shown in Fig. 9b as a function of applied voltage. The peak width is determined by the Scherrer equation $\Delta 2\theta = \lambda/(\tau \cos\theta)$, where τ is a common crystallite for all three diffraction peaks shown in Fig. 9c. The peak widths are convoluted with the measured instrumental resolution. The pseudo-Voigt function corresponds to a linear combination of Gaussian and Lorentzian peak shapes. The shape of the NiO peaks varied between $88 \pm 12\%$ Lorentzian as the experimental sequence progressed, whereas the ITO peaks were about 50% Gaussian. This difference in peaks shape likely reflects the high degree of disorder introduced by the lithium intercalation in the NiO.

The literature value of the NiO lattice constant (JCPDS 47-1049) is 417.71 pm, which is slightly below the range found here (419.2 to 420.4 pm depending on the intercalation state).

The EC mechanism of anodic colored NiO films has been a debated issue. It has been documented in literature that, the coloration process in NiO is a surface phenomenon, most likely occurring in the outer parts of the grains [9]; that is, the coloration is a surface effect and the NiO bulk remains unchanged, independently from the film being bleached or colored [34]. However, according to other literature [10], the active sites for EC reaction in KOH solution are not likely at the surface, but inside the NiO bulk. In order to resolve where the reactions take place, one can check if there are any changes in the lattice constant. In our work, the lattice constant firstly decreases markedly (Fig. 9b) during the coloration process (Ni^{2+}-e^{-}→Ni^{3+}) and then increases back to some degree during the bleaching process (Ni^{3+}+e^{-}→Ni^{2+}). The lattice parameter

changes in Fig. 9b are significant. This is based on the numerical uncertainty of the fitted parameters, shown by the error bars, which do not overlap for the colored and bleached states. More importantly, there is a back-and-forth change of about 0.7 pm for successive coloration steps. In addition, the lattice shrinkage in oxidation of Ni^{2+} to Ni^{3+} and expansion in reversible reduction are in good accordance with the radius of the Ni ions: 0.690 Å (Ni^{2+}) > 0.560 Å (Ni^{3+}) [35]. This effect is more prounounced for △V= ±2.5 V than for △V= ±2.0 V. Repeated measurements at ±2.5 V confirm this result. Since the lattice constant changes upon Li extraction/insertion, we conclude that the coloration/bleaching process is a bulk phenomenon.

On the other hand, the crystallite sizes in Fig. 9c remain constant within the experimental uncertainty. The crystallite sizes of NiO, based on the width of XRD peaks (Scherrer equation), after coloration/bleaching remain near the initial state of ~8 nm (Fig. 9c), in good agreement with the estimated values obtained from the SEM images. No other major differences caused by the applied potential are observed in the error bars. Also, the FWHM of the main Raman peak at 500 cm^{-1} during NiO coloration/bleaching (with Li extraction/insertion) also remains stable at 100 cm^{-1} (Fig. 6) deduced from the deconvolution with LabSpec, which is in good agreement with XRD results. We conclude that the intercalation/deintercalation of Li into the NiO crystallites is a homogeneous process, since otherwise the XRD peak widths would vary. This further supports the notion that intercalation is a bulk process. Thereby, the NiO electrochromism cannot only be a surface process, but the lattice is involved in the charge insertion/extraction.

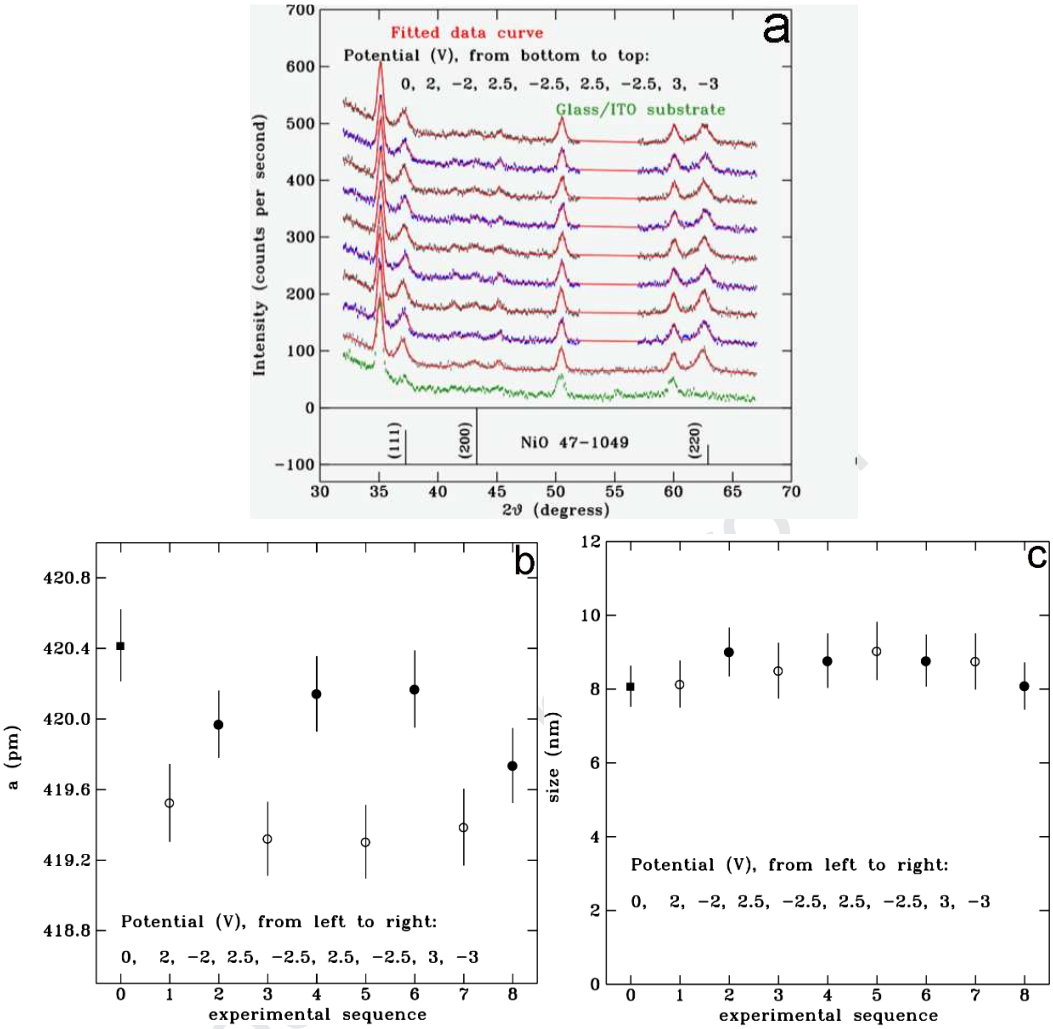

Fig. 9. XRD patterns of NiO a) upon potential cycling, where grey/blue/black lines are experimental points of initial/colored/bleached states and red lines are corresponding to pseudo-Voigt-function fitted curve; b) lattice constants and c) crystallite sizes of NiO deduced from fitted data.

3.3.3 Chronoamperometry

From the optical properties and CIE color measurement, 2.5 V corresponds to the maximum change in EC behavior of NiO, which means the charge insertion/extraction reaches its limit. As a result, when the potential is up to 3.0 V there is no more change in the corresponding lattice constant. Thereby, it is usually recognized that nickel oxide is subjected to a simple two-step electrochemical reaction scheme cycling in Li^+-ion electrolytes [36]:

$$NiO_x + \alpha Li^+ + \alpha e^- \rightarrow Li_\alpha NiO_x, \qquad Li_\alpha NiO_x \rightleftharpoons \gamma Li + \gamma e^- + Li_\beta NiO_x\ (\alpha=\beta+\gamma). \qquad (1)$$

(Initial activation: irreversible) *(Bleached)* *(Colored)*

The transformation between Ni^{2+} and Ni^{3+} correlates with the formation of small polarons in p-type NiO [37]. Increases of the optical absorption by almost one order of magnitude (Fig. S1c&d) can also be explained by the formation of small polarons [32,38]. With this hypothesis, during anodic polarization the dissolution of Ni^{2+} would be possible when the flux of polarons is assisted by the presence of Ni^{3+} while the crystalline NiO structure is maintained, as proved by Raman spectroscopy and XRD.

Chronoamperometry of a NiO film was recorded at ±2.0 V, ±2.5 V and then ±3.0 V with corresponding charge capacities Q calculated from the integral of the current ($Q = \int jdt$) (Fig. 10a). In the matter of the potential increasing to ±3.0 V, the value of Q goes down from coloration to bleaching, and the corresponding curve shape is less sharp in coloration. According to results from Li^+ based batteries, the intercalated Li is lost to the formation of passivating films so capacity decreases [39,40]. On the other hand, in bleaching upon Li^+ ion intercalation, NiO film capacities (Q_1, Q_2 and Q_3) at -2.5 and -3.0 V are stable around 15.9 ± 0.2 C/m^2, which can be used as balanced capacity when the active sites for Li are fully occupied. The lattice constant variation versus inserted Li^+ ions at specified negative potentials for bleaching is depicted (Fig. 10b). The calculation of the ratio γ of mobile L i^+ ions to Ni in coloration/bleaching is based on the following equation:

$$\gamma = \frac{MQ}{\rho h F} \quad (2)$$

where M, Q, ρ, h and F refer to NiO molar mass (7.47×10^{-2} kg/mol), charge capacity (15.9 ± 0.2 C/m^2), NiO density (6670 kg/m^3), film thickness (400 nm) and Faraday constant (9.65×10^4 C/mol), respectively. Here, the average γ is calculated to be around 0.0046, and there is 0.15% lattice shrinkage due to the Li^+ insertion in the bleached state as compared to the initial state at 0V, which is much smaller than 3.3% for WO_3 reported in our previous studies [41]. This is also associated with the structural difference between the relatively dense packing of NiO and much more voids in the tungsten bronze structure.

One Ni atom is in the center of an octahedron formed by six near-neighbor O atoms [42,43]. For one unit cell, there are four nickel and four oxygen atoms (Fig. 10c). Here,

one unit cell (*u.c.*) (a×a×a) contains 8 small cubes with volumes between $(\frac{a}{2})$, $(\frac{a}{2})$, $(\frac{a}{2})$. During bleaching, one Li ion could presumably be inserted at the center of each cube (Fig. 10d) and bring an expansion of the lattice from 419.525 to 419.971 pm at -2V, from 419.321 to 420.17 pm at -2.5V, and from 419.386 to 419.736 pm (see Fig. 9b). The Li sites are half-way between the planes. In Li_xNiO, following the fcc lattice, with standard notation (x, y, z), theoriticaly the fractional coordinates are as listed below.

O-sites: (0, 0, 0), $(\frac{1}{2}, \frac{1}{2}, 0)$, $(\frac{1}{2}, 0, \frac{1}{2})$, $(0, \frac{1}{2}, \frac{1}{2})$

Ni-sites: (0, 0, 0), $(\frac{1}{2}, \frac{1}{2}, 0)$, $(\frac{1}{2}, 0, \frac{1}{2})$, $(0, \frac{1}{2}, \frac{1}{2})$

Li-sites: $(\frac{1}{4}, \frac{1}{4}, \frac{1}{4})$, $(\frac{3}{4}, \frac{1}{4}, \frac{1}{4})$, $(\frac{1}{4}, \frac{3}{4}, \frac{1}{4})$, $(\frac{1}{4}, \frac{1}{4}, \frac{3}{4})$, $(\frac{3}{4}, \frac{3}{4}, \frac{1}{4})$, $(\frac{3}{4}, \frac{1}{4}, \frac{3}{4})$, $(\frac{1}{4}, \frac{3}{4}, \frac{3}{4})$, $(\frac{3}{4}, \frac{3}{4}, \frac{3}{4})$

In this work, based on equation *(2)*, x in Li_xNiO is found to be 0.0046, and it can be defined as the fraction ratio of Li to Ni atoms $(\frac{Li}{Ni})$. Hence, we can evaluate the percentage of Li occupied sites in NiO as follows: $4\frac{Ni}{u.c.} = 0.0184 \approx 2\%$. The maximum number of Li sites in one unit cell is also eight and the maximum ratio of Li/Ni (8/4) is two. However, the actual occupation is much lower and, from the calculated Li/Ni ratio, it can be reckoned that the available space is far from fully accupied. Fraction of unit cell's occupation: $\frac{0.0046Li}{Ni} \times \frac{4Ni/u.c.}{8\ possible\ Li\ sites/u.c.} \approx 2\%\ (\frac{Li}{u.c.})$ or $0.23\%\ \frac{intercalated\ Li}{possible\ Li\ sites}$.

On the other hand, since the NiO film is crystalline, the behavior of Li insertion into one bulk NiO crystallite can also be discussed based on the model proposed by Carl M. Lampert et. al. [10]. The XRD data show one unit cell of closed-packed (*f.c.c.*) NiO with lattice constant around 420 pm and, one crystallite with a dimension around 8 nm, i.e. twenty unit cells on one side. The total number of unit cells in the bulk cube is then calculated to be 8000 and the number of Ni atoms is 32000 (Fig. S2). The ratio of Li/Ni is 0.0046; thereby, the average amount of inserted Li ions into one crystallite is estimated to be 147. That is, there is one Li^+ for every fifty-four unit cells. We notice that this value (0.0046) is much lower than that of WO_3 reported by R.T. Wen et al [44]. where x in Li_xWO_3 exceeds 0.65, for which the structural difference between the relatively dense packing of NiO and much more voids in tungsten bronze structure can also account.

Except charge capacity, coloration efficiency η, which represents the change in the

optical contrast for the charge consumed per unit of electrode area is also a crucial parameter to judge an EC film. It can be evaluated from the formula:

$$\eta = \frac{log(\frac{Tb}{Tc})}{Q} \quad (3)$$

where T_b and T_c refer to transmittance at bleached and colored states, respectively. In this work, for NiO, η is calculated to be ~128cm^2/C ($\frac{log(\frac{80\%}{49.9\%})}{15.9\ cm2/C}$) at 550 nm, which is much higher than the reported η (50cm^2/C) for WO_3 [45]. Higher η in NiO could explain why it is always used as a counter electrode with WO_3 in a full device despite ~~of~~ its lower charge capacity for Li insertion (~16C/m^2).

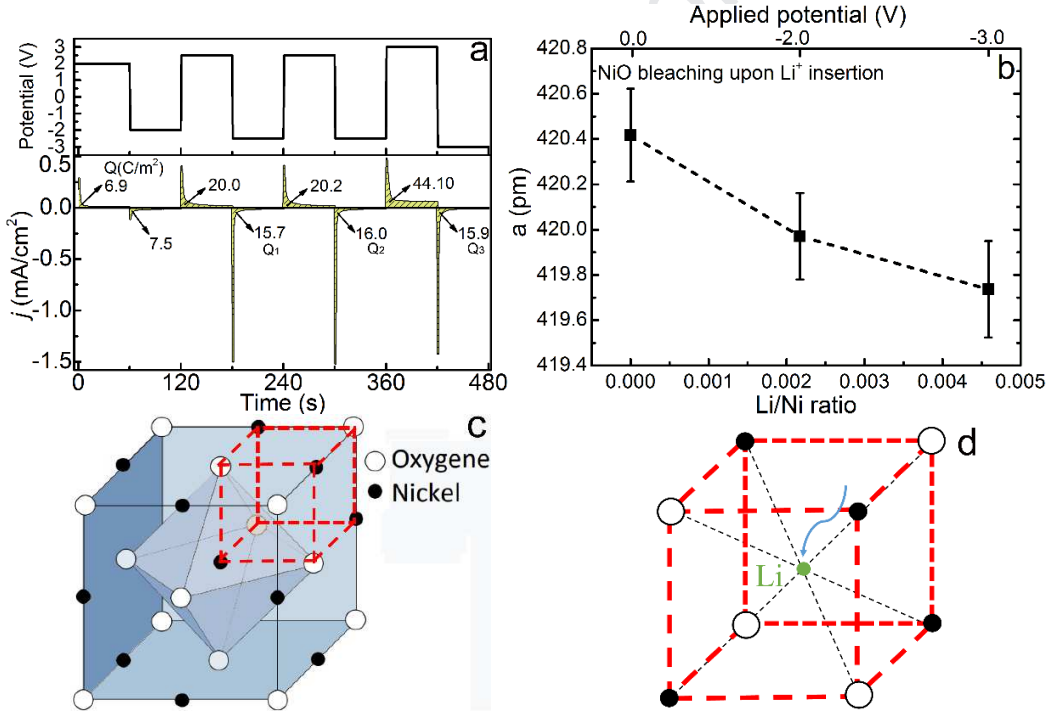

Fig. 10. (a) Chronoamperometry of NiO film recorded at various potentials with calculated charge capacities; (b) lattice constant versus Li^+ ions inserted at the shown potentials and (c) a unit cell of NiO and (d) enlargement of the cube drawn by red dashed line in panel c.

3.4 Electrochemical properties

The cyclic voltammetry on NiO (Fig. 11) films for applied potentials from ±0.5 to ±1.5 V with 5 cycles for each potential is carried out. These experiments are carried out in 1 M $LiClO_4$ at a sweep rate of 100 mV/s. For each sample, the voltammogram changes

with the potential and the number of cycles. An increase in anodic or cathodic current density shows that the reaction increases with the potential window and number of cycles. The charge capacity, deduced from the integral, shown in the inset, exhibits a marked upward trend as the potential range increases. When the potential window is expanded to ±1.5 V, an inconsistency is noted between the 1st cycle and the subsequent ones in the curve shapes, which can be explained by the activation process. For ±1.5 V, the cathodic and anodic peaks observed around +0.05 V, + 0.6 V, -0.13 V and +1.2 V are attributed to the redox reaction involving Ni^{2+}/Ni^{3+} transformation.

In addition, the stability of the ITO electrode working within the potential window is also reflected by the repeatable curves in the cyclic voltammograms at each specific potential, with no peaks appearing or disappearing.

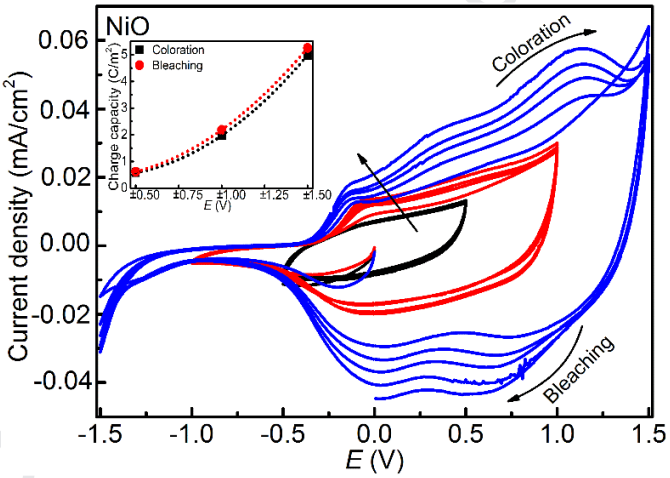

Fig. 11. Cyclic voltammograms of NiO films immersed in $LiClO_4$-PC at enlarging potential windows scanned at 100 mV/s. Insets are the charge capacity.

To study the evolution of charge density of involved ions during the insertion and extraction process as a function of potential, chronoamperometry (CA) was performed at increasing potential steps, for a duration time of 60 s. Figure 12 shows CA plots of potential, together with current density, both as a function of transient time. The accumulative process of charge exchange can be displayed as charge capacity Q (C/m^2) calculated from the integral of the current density curves (see discussion on Fig. 10a above). In switching response, with increasing potential, peak values of current densities are increasing, and more charges participate in the redox reaction (Fig. 12a1&a2).

In modulation (Fig. 12b1&b2), the films become colored in a gradual process, with much more charges exchanged when the potential increases to -1.5 V, which is in agreement with a significant transmittance change (see Fig. 1). However, the bleaching process takes place instantly upon reversing the potential to –0.5V and is associated with a narrow peak that almost completly vanish when the voltage is swept over -1.1 V, respectively (Fig. 12b1). Consequently, the modulation process shows that it is more challenging to get high color saturation than to obtain optical transparency.

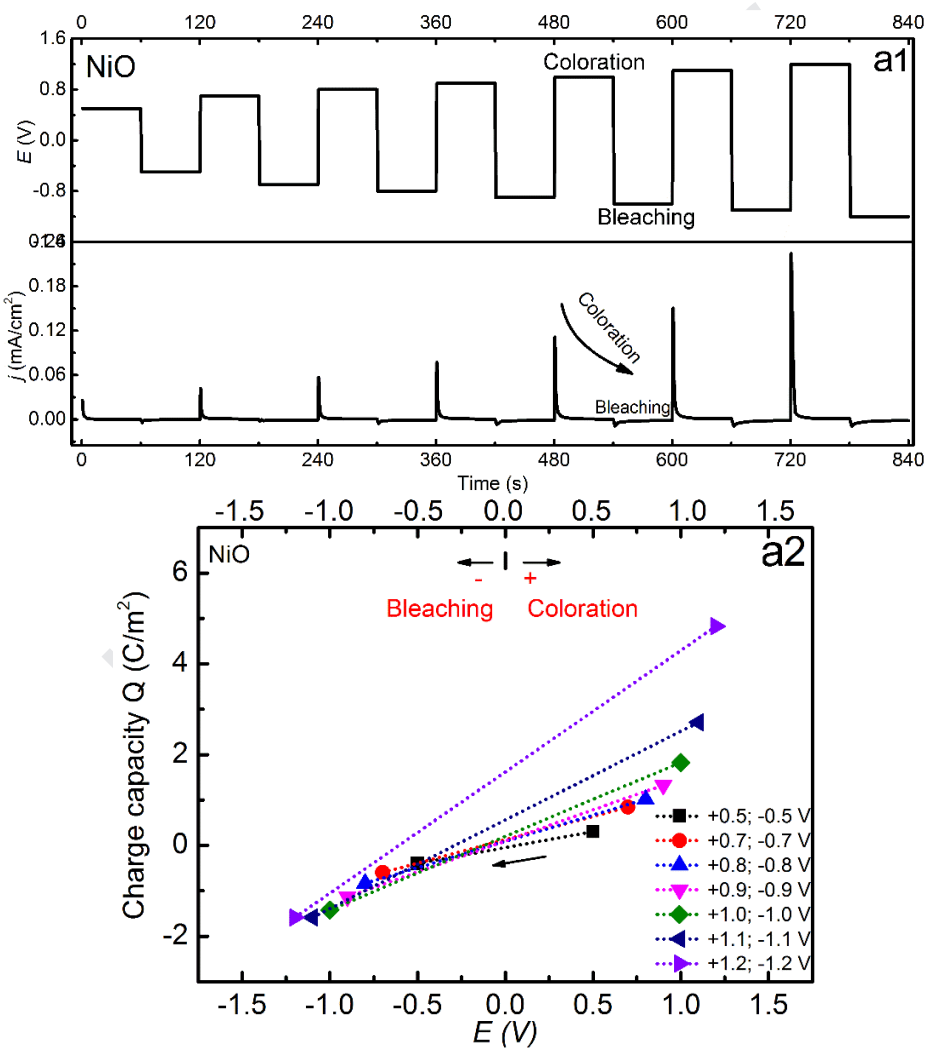

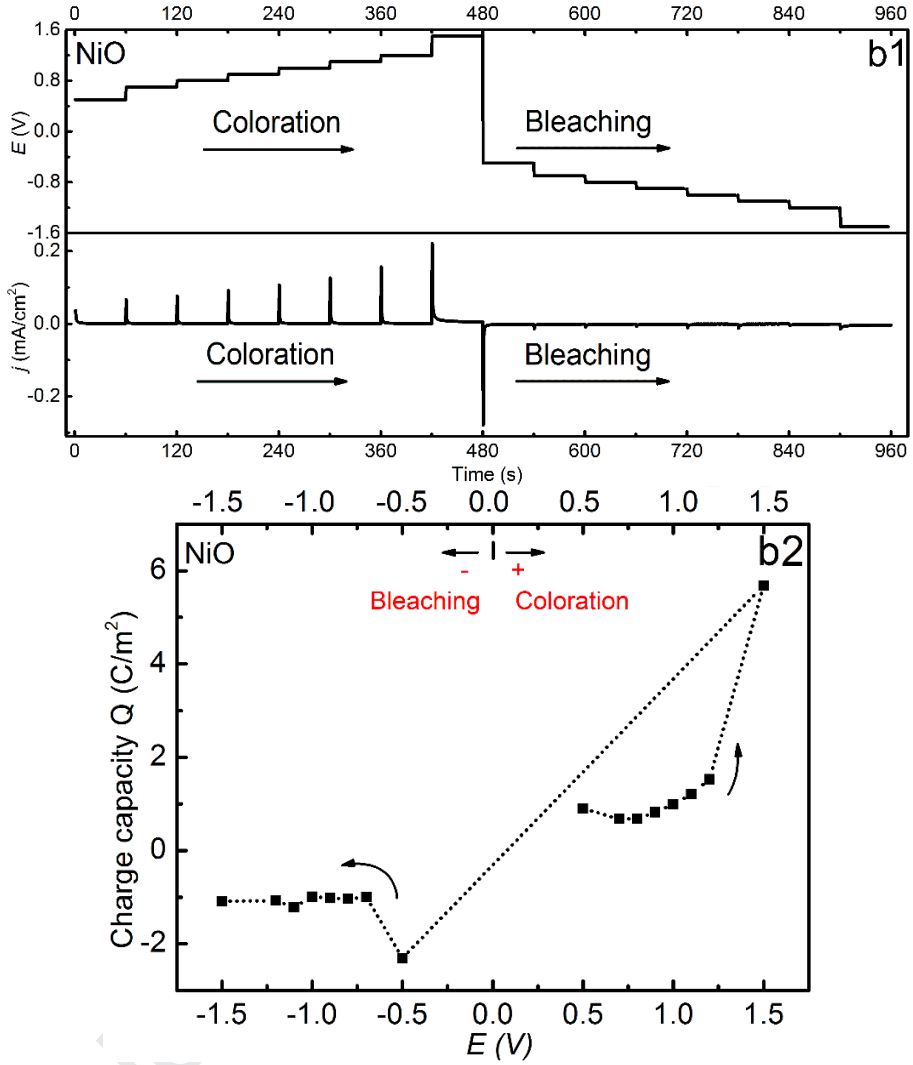

Fig. 12. Chronoamperometry/charge capacity of NiO in switching (a1)/(a2), modulation (b1)/(b2) response immersed in 1 M $LiClO_4$-PC.

4 Conclusion

We present results from a comprehensive electrochromic study of well-characterized sputter-deposited anodic EC NiO films immersed in 1 M $LiClO_4$-PC electrolyte. The optical contrast range is enhanced as voltage is increased, while the increase in coloration is accompanied by a decrease in transmittance. When NiO film is oxidized, a sharp decrease in luminance is observed, as shown by the tracks of the CIE 1931 *xy* chromaticity coordinates. In NiO coloration, a significant red shift of the 512.8 cm^{-1} Raman peak is identified along with new peaks appearing around 926 cm^{-1}. XRD shows a significant increase/decrease in the lattice constant of colored/bleached NiO. This

observation is inconsistent with the hypothesis that NiO electrochromism is only a surface-area limited activity, and this is confirmed by the stability of the FWHM of XRD and Raman peaks. Hence, in this work, it is argued that the inside of the bulk is involved in the Li intercalation reaction process. Also, the x value of the Li_xNiO is calculated to be 0.0046.

Acknowledgements

The financial support of the National Science and Engineering Research Council (NSERC) of Canada ((grant #2017-05094), the John R. Evans Leaders Fund (Canada Foundation for Innovation) (grant #27741), and of the Research Assistantships Initiative of New Brunswick Innovation Fund (NBIF) is gratefully acknowledged. We also think Prof. Sébastien Plante for the use of his MiniScan EZ spectrophotometer.

Conflict of interest

Authors declare no conflict of interest

References

[1] D. M. Dong, W. W. Wang, A. Rougier, A. Barnabe, G. B. Dong, F. Zhang, X. G. Diao, Lithium trapping as a degradation mechanism of the electrochromic properties of all-solid-state WO_3//NiO devices, J. Mater. Chem. C 6 (2018) 9875-9889.

[2] J. S. E. M. Svensson, C. G. Granqvist, Electrochromic hydrated nickel oxide coatings for energy efficient windows: optical properties and coloration mechanism, Appl. Phys. Lett. 49 (1986) 1566-1568.

[3] S. Passerini, B. Scrosati, A. Gorenstein, The intercalation of lithium in nickel oxide and its electrochromic properties, J. Electrochem. Soc. 137 (1990) 3297-3300.

[4] R. T. Wen, G. A. Niklasson, C. G. Granqvist, Electrochromic performance of Ni oxide thin films intercalated with Li^+ ions, J. Phys. Conf. Ser. 559 (2014) 012006.

[5] R. T. Wen, C. G. Granqvist, G. A. Niklasson, Anodic electrochromic nickel oxide thin films: decay of charge density upon extensive electrochemical cycling, ChemElectroChem 3 (2016) 266-275.

[6] H. Moulki, C. Faure, M. Mihelčič, A. Š. Vuk, F. Švegl, B. Orel, G. Campet, M. Alfredsson, A. V. Chadwick, D. Gianolio, A. Rougier, Electrochromic performances of nonstoichiometric NiO thin films, Thin Solid Films 553 (2014) 63-66.

[7] E. Avendaño, A. Azens, G. A. Niklasson, C. G. Granqvist, Proton diffusion and electrochromism in hydrated NiO_y and $Ni_{1-x}V_xO_y$ thin films, J. Electrochem. Soc. 152 (2005) F203-F212.

[8] E. Avendaño, H. Rensmo, A. Azens, A. Sandell, G. D. M. Azevedo, H. Siegbahn, G. A. Niklasson, C. G. Granqvist, Coloration mechanism in proton-intercalated electrochromic hydrated NiO_y and $Ni_{1-x}V_xO_y$ thin films, J. Electrochem. Soc. 156 (2009) 132-138.

[9] G. A. Niklasson, C. G. Granqvist, Electrochromics for smart windows: thin films of tungsten oxide and nickel oxide, and devices based on these, J. Mater. Chem. 17 (2007) 127-156.

[10] A. Agrawal, H. R. Habibi, R. K. Agrawal, J. P. Cronin, D. M. Roberts, Effect of deposition pressure on the microstructure and electrochromic properties of electron-beam-evaporated nickel oxide films, Thin Solid Films 221 (1992) 239-253.

[11] M. Ohring, Substrate surfaces and thin-film nucleation BT-materials science of thin films, 7 (2002) 357-415.

[12] D. M. Mattox, Handbook of physical vapor deposition (PVD) processing, William Andrew 2010.

[13] K. S. Usha, R. Sivakumar, C. Sanjeeviraja, V. Sathe, V. Ganesan, T. Y. Wang, Improved electrochromic performance of a radio frequency magnetron sputtered NiO thin film with high optical switching speed, RSC Adv. 6 (2016) 79668-79680.

[14] M. A. Hassan, C. A. A. Hogarth, A study of the structural, electrical and optical properties of copper tellurium oxide glasses, J. Mater. Sci. 23 (1988) 2500-2504.

[15] K. N. Patel, M. P. Deshpande, V. P. Gujarati, S. Pandya, V. Sathe, S. H. Chaki, Structural and optical analysis of Fe doped NiO nanoparticles synthesized by chemical precipitation route, Mater. Research Bulletin 106 (2018) 187-196.

[16] M. P. Deshpande, K. N. Patel, V. P. Gujarati, K. Patel, S. H. Chaki, Structural, thermal and optical properties of nickel oxide (NiO) nanoparticles synthesized by chemical precipitation method, Adv. Mater. Res. 1141 (2016) 65-71.
[17] X. L. Liu, L. Q. Kong, H. M. Du, Y. Zhang, J. S. Zhao, Y. Xie, Synthesis and electrochromic properties of electrochromic polymers based on propylene dioxythiophene, diketopyrrolopyrrole and benzodithiophene units, Organic Electronics 64 (2019) 223-235.
[18] Y. W. Liang, D. Strohecker, V. Lynch, B. J. Holliday, R. A. Jones, A thiophene-containing conductive metallopolymer using an Fe(II) bis(terpyridine) core for electrochromic materials, ACS Appl. Mater. Interfaces 8 (2016) 34568-34580.
[19] M. Z. Sialvi, R. J. Mortimer, G. D. Wilcox, A. M. Teridi, T. S. Varley, K. U. Wijayantha, C. A. Kirk, Electrochromic and colorimetric properties of nickel(II) oxide thin films prepared by aerosol-assisted chemical vapor deposition, ACS Appl. Mater. Interfaces 5 (2013) 5675-5682.
[20] R. E. Dietz, G. I. Parisot, A. E. Meixner, Infrared absorption and Raman scattering by two-magnon processes in NiO, Phys. Rev. B 4 (1971) 2302-2310.
[21] J. C. Lai, X. C. Wang, W. B. Mi, Y. H. Ding, B. H. Yang, Structure and optical properties of polycrystalline NiO films and its resistive switching behavior in Au/NiO/Pt structures, Physica B: Condensed Matter 478 (2015) 89-94.
[22] K. Kaviyarasu, E. Manikandan, J. Kennedy, M. Jayachandran, R. Ladchumananandasiivam, U. U. De Gomes, M. Maaza, Synthesis and characterization studies of NiO nanorods for enhancing solar cell efficiency using photon upconversion materials, Ceramics International 42 (2016) 8385-8394.
[23] V. Biju, M. A. Khadar, Fourier transform infrared spectroscopy study of nanostructured nickel oxide, Spectrochim. Acta A: Mol. Biomol. Spectrosc. 59 (2003) 121-134.
[24] M. Che, A. J. Tench, Characterization and reactivity of molecular oxygen species on oxide surfaces, Adv. Catal. 32 (1983) 1-148.
[25] S. A. Mahmoud, A. A. Akl, H. Kamal, K. Abdel-Hady, Opto-structural, electrical and electrochromic properties of crystalline nickel oxide thin films prepared by spray pyrolysis, Physica B: Condensed Matter 311 (2002) 366-375.
[26] N. Mironova-Ulmane, A. Kuzmin, I. Steins, J. Grabis, I. Sildos, M. Pärs, Raman scattering in nanosized nickel oxide NiO, J. Phys. 93 (2007) 012039.
[27] R. E. Dietz, W. F. Brinkman, A. E. Meixner, H. J. Guggenheim, Raman scattering by four magnons in NiO and $KNiF_3$, Phys. Rev. Lett. 27 (1971) 814.
[28] L. De Los Santos Valladares, A. Ionescu, S. Holmes, C. H. Barnes, A. Bustamante Dominguez, O. Avalos Quispe, J. C. González, S. Milana, M. Barbone, A. C. Ferrari, H. Ramos, Characterization of Ni thin films following thermal oxidation in air, J. Vac. Sci. Technol. B 32 (2014) 051808.
[29] Y. L. Lo, B. J. Hwang, In situ Raman studies on cathodically deposited nickel hydroxide films and electroless Ni-P electrodes in 1 M KOH solution, Langmuir 14 (1998) 944-950.
[30] H. Y. Qu, D. Primetzhofer, Z. Qiu, L. Österlund, C. G. Granqvist, G. A. Niklasson, Cation-/anion-based electrochemical degradation and rejuvenation of electrochromic nickel oxide thin films, ChemElectroChem 5 (2018) 3548-3556.
[31] X. Cao, Y. Shi, W. Shi, G. Lu, X. Huang, Q. Yan, Q. Zhang, H. Zhang, Preparation of novel 3D graphene networks for supercapacitor applications, Small 7 (2011) 3163-3168.
[32] S. I. Cordoba-Torresi, A. Hugot-Le Goff, S. Joiret, Electrochromic behavior of nickel oxide electrodes II. identification of the bleached state by Raman spectroscopy and nuclear reactions, J. Electrochem. Soc. 138 (1991) 1554-1559.
[33] N. Mironova-Ulmane, A. Kuzmin, I. Steins, J. Grabis, I. Sildos, M. Pärs, Raman scattering in nanosized nickel oxide NiO, J. Phys. Conf. Ser. 93 (2007) 012039.
[34] N. Nakajima, H. Kato, Y. Sakisaka, Surface metallic nature caused by an in-gap state of reduced NiO: a photoemission study, J. Electron Spectroscopy, Related Phenomena 144 (2005) 873-875.
[35] G. Leftheriotis, S. Papaefthimiou, P. Yianoulis, The effect of water on the electrochromic properties of WO_3 films prepared by vacuum and chemical methods, Sol. Energy Mater. Sol. Cells 83 (2004) 115-124.
[36] Q. Liu, Q. Chen, Q. Zhang, Y. Xiao, X. Zhong, G. Dong, M. P. Delplancke-ogletree, H. Terryn, K. Baert, F. Reniers, X. Diao, In situ electrochromic efficiency of a nickel oxide thin film: origin of electrochemical process and electrochromic degradation, J. Mater. Chem. C 6 (2018) 646-653.
[37] E. Iguchi, K. Akashi, Dielectric relaxation and electrical transport due to nonadiabatic small polarons in P-type NiO doped with Li, J. Phys. Soc. Japan 61 (1992) 3385-3393.
[38] I. G. Austin, B. D. Clay, C. E. Turner, A. J. Springthorpe, Near and far infrared absorption by small polarons in semiconducting NiO and CoO, Solid State Commun. 6 (1968) 53-56.
[39] E. Peled, D. Golodnitsky, G. Ardel, Advanced model for solid electrolyte interphase electrodes in liquid and polymer electrolytes, J. Electrochemical Soc. 144 (1997) 208-210.
[40] E. Peled, The electrochemical behavior of alkali and alkaline earth metals in nonaqueous battery systems—the solid electrolyte interphase model, J. Electrochemical Soc. 126 (1979) 2047-2051.
[41] S. Balaji, Y. Djaoued, A. S. Albert, R. Z. Ferguson, R. Bruning, Hexagonal tungsten oxide based electrochromic

devices: spectroscopic evidence for the Li ion occupancy of four-coordinated square windows, Chem. Mater. 21 (2009) 1381-1389.

[42] S. V. Green, M. Watanabe, N. Oka, G. A. Niklasson, C. G. Granqvist, Y. Shigesato, Electrochromic properties of nickel oxide based thin films sputter deposited in the presence of water vapor, Thin Solid Films 520 (2012) 3839-3842.

[43] D. M. Dong, W. W. Wang, G. B. Dong, Y. L. Zhou, Z. H. Wu, M. Wang, F. M. Liu, X. G. Diao, Electrochromic properties of NiO_x:H films deposited by DC magnetron sputtering for ITO/NiO_x:H/ZrO_2/WO_3/ITO device, Appl. Surf. Sci. 357 (2015) 799-805.

[44] R. T. Wen, C. G. Granqvist, G. A. Niklasson, Eliminating Degradation and Uncovering Ion-Trapping Dynamics in Electrochromic WO_3 Thin Films, Nature Mater. 14 (2015) 996.

[45] D. M. Dong, W. W. Wang, A. Rougier, G. B. Dong, M. Da Rocha, P. Lionel, K. Zrikem, G. Song, X. G. Diao, A. Barnabé, Life-cycling and uncovering cation-trapping evidence of a monolithic inorganic electrochromic device: glass/ITO/WO_3/$LiTaO_3$/NiO/ITO, Nanoscale 10 (2018) 16521-16530.

CRediT author statement

Dongmei Dong: Conceptualization, Methodology, Investigation, Discussion, writing, and reviewing; **Habiba Djaoued:** Participation in the Colorimetric studies**; Guillaume Vienneau**: Participation in the electrochemical characterization; **Jacques Robichaud**: Raman and SEM characterization, Writing/Reviewing; **Delilah Brown**: XRD characterization; **Ralf Brüning**: XRD writing, discussion and reviewing; **Yahia Djaoued**: Conceptualization, Methodology, Investigation, Discussion, Writing, Reviewing and Editing

Declaration of interests

☒ The authors declare that they have no known competing financial interests or personal relationships that could have appeared to influence the work reported in this paper.

☐The authors declare the following financial interests/personal relationships which may be considered as potential competing interests: